Fluid Dynamics &
Materials Processing

Tech Science Press

http://doi.org/10.32604/fdmp.2026.083469

ARTICLE

Optimizing Hollow Block Roof Design: A Numerical Investigation of Coupled Heat Transfer under Solar Radiation

Ayoube Baalla*, **Mourad Najjaoui, Thami Ait-Taleb and Hassan Chaib**

Materials and Energy Research Team, Polydisciplinary Faculty of Ouarzazate, Ibn Zohr University, Ouarzazate, Morocco
*Corresponding Author: Ayoube Baalla. Email: ayoube.baalla@edu.uiz.ac.ma

Received: 04 April 2026; Accepted: 14 July 2026; Published: 31 July 2026

ABSTRACT: The complex interplay of heat transfer mechanisms, namely conduction, natural convection, and radiation, within hollow block roofs exposed to solar irradiation gives rise to an inherently nonlinear thermal exchange problem. A key yet insufficiently explored question is the extent to which this nonlinearity governs the macroscopic thermal behavior of roofing systems. In this study, a computational investigation is conducted on two roof configurations incorporating five hollow block geometries representative of common construction practices in hot climatic regions. The objective is to identify the optimal design capable of minimizing heat losses and thereby enhancing the overall thermal performance of buildings. The outer roof surfaces are subjected to terrestrial solar radiation and convective exchange with the outdoor environment, whereas the inner surfaces interact with indoor ambient conditions. The governing partial differential equations and associated boundary conditions are discretized using the finite volume method in conjunction with the SIMPLE algorithm. Particular attention is devoted to examining the effects of solar radiation intensity, solid wall thermal conductivity, and cavity aspect ratio on fluid flow characteristics and heat transfer across the roof structures. The results highlight the critical importance of incorporating solar radiation effects into roof design.

KEYWORDS: Heat transfer; computational study; solar radiation; hollow block; thermal conductivity; aspect ratio

1 Introduction

Buildings account for approximately 36% of total energy consumption, of which residential buildings contribute about 29%, with the remainder allocated to tertiary buildings [1]. The future landscape anticipates a substantial upswing in energy consumption, propelled by the robust expansion of the building sector and the diminishing costs of heating and cooling equipment. This imminent concern has spurred designers to explore viable solutions aimed at curtailing the thermal loads linked to air conditioning. The building envelope, encompassing walls, floors, and windows, plays a pivotal role. Among these components, walls and floors stand out as significant sources of thermal energy exchange. Notably, the roof emerges as the building envelope element most susceptible to weather effects, contributing to 30% of thermal exchange in Morocco [2]. Therefore, it becomes imperative to meticulously evaluate the thermal performance of building roofs to optimize heat gains or losses. Hollow concrete blocks are widely used as roofing materials, thanks to their manifold advantages, including thermal efficiency, lightweight characteristics, and cost-effectiveness. Typically, these structures involve intertwined heat transfers facilitated by natural convection within cavities, conduction across solid partitions, and the exchange of thermal radiation occurring on the faces of the cavities.

Recent studies have undertaken numerous investigations to scrutinize the combined heat exchange mechanisms within hollow structures [3–7]. These investigations have provided valuable insights into the interplay of various heat exchange modes, encompassing flow fields, temperature distribution, and heat transfer within the studied structures. Remarkable alterations have been observed, particularly in the presence of radiation. Gossard and Lartigue [8], alongside Sambou et al. [9], delved into the phenomenon of conjugate heat transfer in enclosures with thick conductive partitions, exploring variables such as thermal conductivity ratio, the number of partitions, and void fraction's impact on heat transfer. The broader literature on solar-coupled thermal systems further contextualises the present work. Within this broad class of coupled CFD heat-transfer analyses, Majeed et al. [10] examined flow and heat transfer over a pair of heated bluff bodies in a channel governed by non-linear rheological models, revealing the strong sensitivity of the coupled thermal field to the governing flow parameters. Iqbal et al. [11] investigated hybrid nanofluid flow in a Parabolic Trough Solar Collector (PTSC) integrated within solar-powered aircraft wings, demonstrating through coupled numerical and ANN-based modelling that the radiation parameter carries the highest sensitivity on thermal transport a finding that underscores the importance of correctly resolving radiative contributions in any solar-exposed thermal system, including building roofs. In a related study, Akbar et al. [12] extended the PTSC-wing configuration to a Darcy–Forchheimer porous medium framework, showing that hybrid nanofluids boost collector thermal efficiency by up to 4.5% and that the Brinkman number is the dominant parameter governing thermal performance; their use of local non-similarity methods with ANN validation reinforces the value of combining physics-based and data-driven approaches when multiple competing transport mechanisms are present. Makinde et al. [13] modelled solar steam desalination using a copper-sulphide-infused selective porous solar absorber embedded in a Darcy–Forchheimer porous matrix, showing that the absorber Biot number governs the interfacial heat flux and Nusselt number, while increasing the CuS volume fraction thins the thermal boundary layer and enhances steam generation. In a separate study, Antar [14] analyzed coupled heat exchange in construction blocks with multiple cavities, revealing a significant reduction in heat flux with an increase in the number of holes. Nouanegue et al. [15] conducted a numerical investigation into heat transfer modes within an inclined cavity exposed to uniform heat flux. Their findings unveiled a notable coupling effect among these mechanisms, further accentuated by the influence of radiation. Gao et al. [16] developed a simulation model incorporating phase change heat transfer, demonstrating a substantial reduction in heat flux through the incorporation of phase change materials (PCM). Additionally, Chihab et al. [17] investigated combined heat transfer with real thermal excitations in a hot urban climate. Their study emphasized the noteworthy impact of heat transfer coefficients associated with radiation and convection on the thermal inertia of roofs. Furthermore, Xamán et al. [18] delved into the investigation of hollow bricks for roofs, factoring in environmental variables and the application of insulation materials and sun-reflective coatings. Their findings underscored the advantages of incorporating insulation and reflective coatings, particularly in warm climates. In a separate numerical investigation, Jamal et al. [19] explored heat transfer within a wall constructed with hollow bricks, revealing the significant influence of solar radiation on the heat transfer process in the exposed wall. The same authors [20] extended their study to double solid layer walls separated by an air gap layer exposed to solar radiation, concluding that selecting an optimal air gap thickness can lead to reduced energy consumption in buildings. Moreover, research has been conducted to explore the most efficient cavity geometry for enhancing the heat insulation capabilities of hollow blocks [21,22]. Morales et al. [23] conducted a numerical investigation with the aim of enhancing the geometric arrangement of walls constructed using hollow clay bricks to optimize their thermal efficiency. In a study by Sun and Fang [24], the heat transfer behavior of hollow bricks with various structures was examined, specifically focusing on the impact of enclosure geometry with the same void volume fraction. They also investigated the effects of staggered enclosures. Al-Tamimi et al. [25] explored the impact of cavity geometry on heat transfer in concrete bricks, revealing that rectangular cavities exhibited higher thermal efficiency compared to circular shapes. Santos et al. [26] determined the thermal transmittance of different concrete bricks, highlighting that blocks with larger cavities facilitated increased airflow, resulting in higher coefficients of convective heat transfer and consequently higher thermal transmittance. Additionally, Najjaoui et al. [27] presented a computational study on the combined effects of the three modes of heat exchange in commonly used hollow structures for building ceilings and investigated the impact of hole configuration. Their findings revealed that holes with a high aspect ratio led to a substantial reduction in heat exchange through the hollow block, achieving an approximately 14% improvement in thermal performance. JJ del Coz Díaz [28,29] employed numerical simulations to investigate heat exchange in various types of bricks, identifying the optimal structure for hollow roofs with superior thermal efficiency. In a study conducted by Sassine et al. [30], the impact of block geometry on global thermal resistance was examined to enhance the heat efficiency of hollow blocks in Lebanon. Additionally, several studies [31–33] have explored the influence of thermal conductivity on the thermal resistance of the cellular components of buildings. The results unveiled a significant influence of thermal conductivity on the global heat exchange within the system. Accordingly, reducing the conductivity of the block was found to enhance the overall thermal resistance. Antoniadis et al. [33] analyzed and measured the conductivity of clay bricks in Greece. They introduced a novel design that improved the thermal performance of these bricks by an impressive 24%. More recent numerical and experimental studies have continued to refine this understanding: hollow concrete blocks commonly used in Morocco have been assessed and improved through combined experimental–numerical approaches [34]; phase-change material integrated into lightweight hollow-concrete roofs has been shown to attenuate peak heat fluxes in warm climates [35]; the thermal conductivity of insulated hollow blocks has been optimised for hot-climate service [36]; multi-physics finite-element analyses have guided the design of eco-sustainable hollow-brick mixes [37]; and reflective, super-cool and temperature-adaptive roof strategies have been reviewed as passive means of limiting solar heat gain [38].

The two closest antecedents to the present work are Najjaoui et al. [27] and Xamán et al. [18], yet each leaves a distinct and consequential gap. Najjaoui et al. [27] investigated the effect of hole configuration and, separately, thermal conductivity on heat exchange in a single, representative hollow block subjected to solar flux; their findings established the importance of aspect ratio and conductivity in isolation, but did not compare multiple commercially available multi-cellular roof configurations against one another under the same climatic boundary conditions, nor did they interrogate whether the three-mode coupling produces a linear or nonlinear global thermal response. Xamán et al. [18], working on hollow bricks, evaluated the benefit of insulating coatings and reflective materials on a single block geometry; their study is therefore geometry-specific, climate-specific to a single region, and focused on add-on treatments rather than on the intrinsic structural hierarchy of the block itself. Before stating the guiding research question, it is necessary to be explicit about where the novelty of this study lies, since the work combines three elements that could each be mistaken for the primary contribution. The use of hollow-block geometries (two roof configurations, five block types drawn from the regional market) constitutes a contextual novelty: these specific multi-cellular configurations, which are widely used in hot-climate construction practice, have not previously been studied in direct comparison under identical boundary conditions. The numerical scheme utilized (finite volume discretization along with the SIMPLE algorithm and radiosity heat transfer model that solves the problem of all three heat transfer mechanisms simultaneously) is an already recognized technique. However, its use on the specific geometrical configurations is new but is not a breakthrough from a scientific point of view since it does not offer anything fundamentally new. The parametric study of the global heat flux depending on such parameters as solar irradiation, solid conductivities, and cavity aspect ratio offers a more complete approach to the problem compared to previous work that considered only one parameter at a time. The primary scientific novelty is the mechanistic finding that emerges from this combination: despite the strongly nonlinear radiative–conductive coupling within the cavities, the macroscopic heat flux responds nearly linearly to solar irradiance, because solid-partition conduction dominates the global thermal pathway and short-circuits the cavity-level nonlinearity. This hierarchy and its geometric consequence, namely that vertical cavity stratification is the most effective structural lever for thermal resistance, is the result that prior studies of individual block geometries could not have revealed, and it is this finding that provides transferable physical understanding beyond any single regional context. Neither study addressed the following mechanistic question, which this investigation is designed to answer: Does the strongly nonlinear radiative–conductive coupling within hollow-block cavities govern the macroscopic heat flux through the roof, or does solid-partition conduction dominate and impose an effectively linear global response and how does the answer depend on the number and vertical arrangement of cavities in configurations that are widely used in hot-climate construction? This guiding question threads through the entire study: the numerical model is constructed to resolve all three coupled modes simultaneously across five block geometries under representative hot-climate climatic excitations; the results are interpreted primarily in terms of which mechanism dominates and why; and the design recommendations follow directly from the mechanistic hierarchy revealed, rather than from empirical optimisation alone.

2 Analysis

2.1 Defining the Problem Statement

The studied system, depicted in Fig. 1, consists of alveolar roofs. The top surface faces is under solar radiation and ambient temperature (T_{out}), with a convective heat transfer coefficient (h_{out}). The inner side is exposed to the temperature within the indoor space (T_{in}) and a convective heat exchange coefficient (h_{in}). Adiabatic conditions are assumed for the vertical surfaces.

Five types of floor-building units were chosen based on an inquiry into the most used blocks in constructing building roofs in hot-climate regions [39]. These blocks, known as “hourdis” are illustrated in Figs. 2–4, representing concrete hollow blocks. They feature a honeycomb structure formed by one or two deep air cells vertically and 3 or 4 identical holes horizontally.

(**a**)

Figure 1: *Cont.*

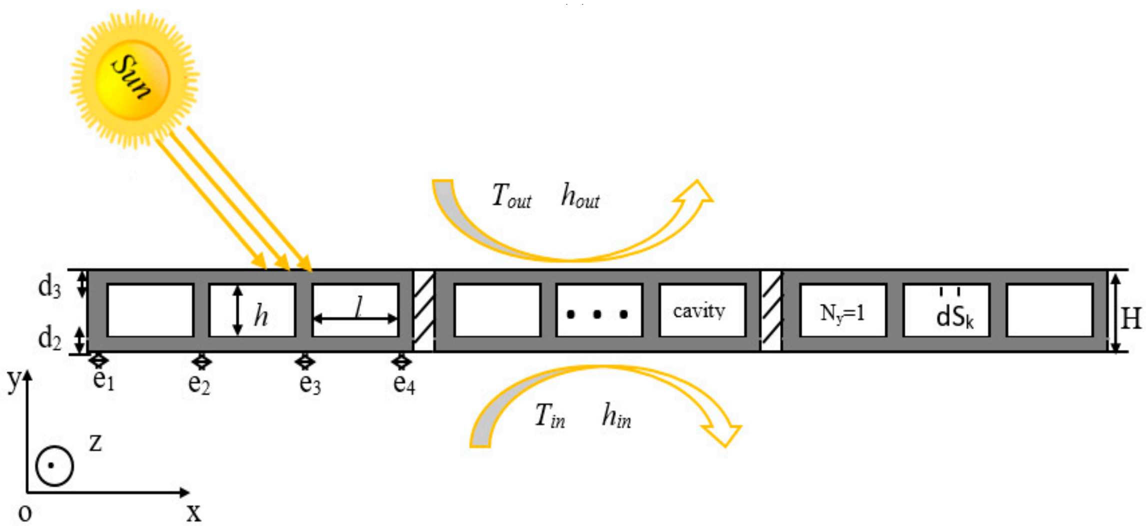

(**b**)

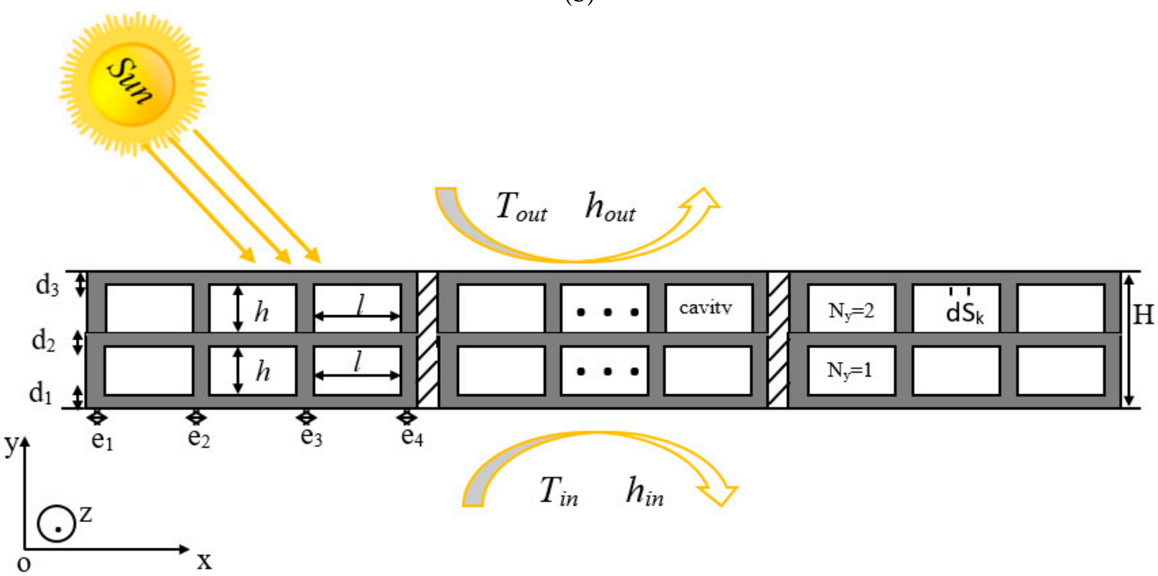

(**c**)

Figure 1: Studied system: (**a**) hollow block roofs; (**b**) Physical model Type 1 and (**c**) Physical model Type 2.

Figure 2: Hollow block with 8 × 20 × 52 cm^3 (H1) and 20 × 20 × 52 cm^3 (H2) dim.

Figure 3: Hollow block with 12 × 25 × 52 cm^3 (H3) and 16 × 25 × 52 cm^3 (H4) dim.

Figure 4: Hollow block with 25 × 20 × 52 cm^3 (H5) dim.

The heat exchange process across the cavities (holes) of the hollow structure is a complex phenomenon that entails the coupling of natural convection within the inner holes, heat conduction through solid partitions, and radiation between the sides of the inner cavities. Consequently, the overall heat exchange through these perforations exhibits distinct nonlinear characteristics. To express this problem mathematically, the following assumptions have been made:

- The problem is steady and two-dimensional.
- Viscous dissipation is considered negligible.
- The fluid and solid properties are assumed to be constant throughout, except for the density variation in the buoyancy term, where the Boussinesq approximation holds.
- The fluid is considered non-participating in radiation, and the surfaces inside the cavities are assumed to be diffuse gray.

2.2 Model Limitations

While the present model provides valuable insights into the thermal behavior of Moroccan hollow blocks, certain limitations should be acknowledged. First, the 2D heat and fluid flow steady-state assumption which is dictated by the disposition of the hollow tiles in the construction of building roofs (see photo and figures above). In the practice, the hollow tile is placed in such a way that the length of the internal cavities in the direction (Oz) as channels aligned, very deep in the z direction (in the vicinity 10 m: building length) is infinite compared to the width l (l ≈ 13 cm) in (Ox) direction and to the height h (h ≈ 3.5 cm) in the (Oy) direction. So this assumption neglects three-dimensional edge effects and the thermal inertia of the roof under transient real-world weather conditions, which might lead to a slight overestimation of instantaneous heat fluxes. Second, assuming constant thermophysical properties and a simplified energy model (Boussinesq approximation which consists of neglecting the variations of the air density with the temperature everywhere except in the buoyancy term which is adopted. Thus, the fluid density in the term that generates the movement), so it does not account for the temperature-dependency of material conductivity over wide thermal ranges. Finally, while the adiabatic boundary conditions on vertical faces simulate a periodic pattern in large roof surfaces, they do not capture the lateral heat bridges present at the junctions with supporting beams. Despite these simplifications, the model remains a robust and computationally efficient tool for the comparative thermal characterization of different alveolar structures.

2.3 Mathematical Equations

Using the hypotheses put forth earlier and considering the conservation equations of mass, momentum, and energy in a steady state, a mathematical formulation is constructed using the following set of equations:

$$\frac{\partial U}{\partial X} + \frac{\partial V}{\partial Y} = 0 \tag{1}$$

$$\frac{\partial U}{\partial \tau} + U\frac{\partial U}{\partial X} + V\frac{\partial U}{\partial Y} = -\frac{\partial P}{\partial X} + \Pr(\frac{\partial^2 U}{\partial X^2} + \frac{\partial^2 U}{\partial Y^2}) \tag{2}$$

$$\frac{\partial V}{\partial \tau} + U\frac{\partial V}{\partial X} + V\frac{\partial V}{\partial Y} = -\frac{\partial P}{\partial Y} + \Pr(\frac{\partial^2 V}{\partial X^2} + \frac{\partial^2 V}{\partial Y^2}) + Ra.\Pr.\theta_f \tag{3}$$

$$\frac{\partial \theta_f}{\partial \tau} + U\frac{\partial \theta_f}{\partial X} + V\frac{\partial \theta_f}{\partial Y} = \frac{\partial^2 \theta_f}{\partial X^2} + \frac{\partial^2 \theta_f}{\partial Y^2} \tag{4}$$

The equation for conduction heat transfer in solid materials:

$$\frac{\alpha_f}{\alpha_s}\frac{\partial \theta_s}{\partial \tau} = \frac{\partial^2 \theta_s}{\partial X^2} + \frac{\partial^2 \theta_s}{\partial Y^2} \tag{5}$$

The numerical study employs the following thermal boundary conditions:

- Adiabaticity conditions are applied at the vertical faces:

$$\left(\frac{\partial \theta_s}{\partial X}\right)_{X=0} = \left(\frac{\partial \theta_s}{\partial X}\right)_{X=1} = 0 \quad 0 \le Y \le 1 \tag{6}$$

- For the external horizontal side in contact with the outer environment:

$$\frac{H}{k_s \Delta T}\alpha.S + \frac{h_{out}H}{k_s}(\theta_{out} - \theta s_{out}) = \frac{d\theta s}{dY} \tag{7}$$

- For the interior horizontal side in contact with the inside ambient:

$$\frac{h_{in}H}{k_s}(\theta s_{in} - \theta_{in}) = \frac{d\theta s}{dY} \tag{8}$$

- Continuity of temperature and heat flow in solid-fluid interfaces:

$$\theta_s(X, Y) = \theta_f(X, Y) \tag{9}$$

$$-\frac{\partial \theta_s}{\partial \eta} = -N_k \frac{\partial \theta_f}{\partial \eta} + N_r Qr \tag{10}$$

The radiative heat flux $q_{r,k}(r_k)$ is determined using the following radiosity approach [40]:

$$q_{r,k}(r_k) = J_k(r_k) - E_k(r_k) \tag{11}$$

where $E_k(r_k)$ is the incident radiative heat flux and $J_k(r_k)$ is the radiosity on the surface field given respectively by:

$$J_k(r_k) = \varepsilon_k \sigma (T_k(r_k))^4 + (1-\varepsilon_k) E_k(r_k) \tag{12}$$

$$E_k(r_k) = \sum_{j=1}^{4} \int_{A_j} J_j(r_j) dF_{dS_k - dS_j(r_k, r_j)} \tag{13}$$

The dimensionless net radiative flux exchanged by the surface element dS_k located at a point of abscissa r_k on the side (k) can be expressed as:

$$Q_{r,k}(r_k') = \varepsilon_k \left(\left| 1 - \frac{T_{in}}{T_{out}} \right| \theta_k(r_k') + \frac{T_{in}}{T_{out}} \right)^4 - \varepsilon_k \sum_{j=1}^{4} \int_{S_j} J_j'(r_j') dF_{dS_k - dS_j} \tag{14}$$

The dimensionless average heat flux across the structure is given by:

$$Q_a = -\frac{H}{L} \int_0^{\frac{L}{H}} \left. \frac{d\theta_S}{dY} \right)_{Y=0} dX = -\frac{H}{L} \int_0^{\frac{L}{H}} \left. \frac{d\theta_S}{dY} \right)_{Y=1} dX \tag{15}$$

This equation calculates the dimensional average heat flux in ($W \cdot m^{-2}$):

$$Q = (Q_a \times k_s \times \Delta T)/H \tag{16}$$

The dimensionless stream function Ψ is defined as:

$$\mathrm{U} = -\frac{\partial \Psi}{\partial \mathrm{Y}} \quad \text{and} \quad \mathrm{V} = \frac{\partial \Psi}{\partial \mathrm{X}} \tag{17}$$

The finite volume method, developed by Patankar [41], has been employed to solve the differential equations governing conjugate heat transfer. The numerical calculations were performed by coupling the continuity and momentum equations using a power law scheme and were solved by the SIMPLE algorithm The resulting system of algebraic equations is solved by the Tri-Diagonal-Matrix-Algorithm. Based on this a custom FORTRAN code has been developed and implemented.

Before using this code, the validity of the numerical code was checked. In fact, the obtained results were compared with those of Akiyama and Chong [42], who studied the effect of radiation on natural convection in a differentially heated square cavity. The convective Nusselt numbers calculated at the hot wall are compared in Table 1 for an arrange of Rayleigh number $103 \le \mathrm{Ra} \le 106$ and for different values of the emissivity. The comparative results show an excellent agreement, with a maximum deviation of 0.9%.

Table 1: Comparison of the mean convective Nusselt number for different values of Rayleigh.

	ε = 0.0				ε = 1.0			
Ra	10^3	10^4	10^5	10^6	10^3	10^4	10^5	10^6
Akiyama and Chong	1.125	2.250	4.625	9.375	1.250	2.250	4.250	8.125
Present code	1.119	2.255	4.632	9.462	1.250	2.246	4.271	8.118

3 Results and Discussion

The findings presented in this investigation arise from an analysis conducted on hollow block roofs. The geometric parameters of the structures studied are given in Table 2. The emissivity of the internal walls is taken to be equal to 0.9. The conductivity of the solid material k_s ranges from 0.5 to 1.5 ($0.5 \leq k_s \leq 1.5$). The fluid within the cavities is air with a Prandtl number of Pr = 0.71, with a thermal conductivity of k_f = 0.0262 W/mK, and a thermal diffusivity of $\alpha_f = 1.57 \times 10^{-5}$ m^2/s. The incident solar irradiance (S) fluctuates between 0 and 1000 W/m^2 (0 W/m$^2 \leq S \leq$ 1000 W/m^2). The convective heat exchange coefficients at the indoor and outdoor sides are given respectively by h_{in} = 8.3 W/m^2 $^\circ$C and h_{out} = 17 W/m^2 $^\circ$C, all these values are taken as standard surface heat-transfer values from the ASHRAE Handbook of Fundamentals [43]. The outdoor air temperature is regulated at T_{out} = 40°C, and the temperature of the indoor is fixed to T_{in} = 20°C. These thermal conditions establish a significant temperature gradient across the roof, driving a complex competition between the three modes of heat transfer. The physical superiority of certain designs, such as Type 2 and H5, will be interpreted based on their ability to maximize the solid-to-void thermal resistance and limit the intensity of buoyancy-driven flows within the air cells, effectively acting as thermal dampers against the high incident solar flux.

Table 2: Geometrical dimensions of the studied system.

Model	l (m)	h (m)	e_x (m)	e_y (m)	Number of Cavities
H1	0.14	0.06	0.025	0.02	3
H2	0.14	0.16	0.025	0.02	3
H3	0.1	0.08	0.025	0.02	4
H4	0.1	0.12	0.025	0.02	4
H5	0.14	0.085	0.025	0.02	6

In steady state conditions, the effect of grid spacing on the results of (Ψ_{max} and Q) has been examined by using a non-uniform grid of 305 × 20; 305 × 30, 305 × 40 for Type 1 roofs (H1). Table 3 below illustrates this effect on the solution obtained for the value of $\Delta T = T_{out} - T_{in}$ = 20°C, emissivity ε = 0.9 and thermal conductivity k = 1 W/mK and for the solar radiation S = 0 W/m^2 and S = 1000 W/m^2. As it's shown that the grid 305 × 30 is widely sufficient for modelling correctly the heat transfer and the fluid flow inside the cavities of the hollow block. For Type 2 roofs (H2), in Table 4 demonstrate the improved performance with a grid size of 305 × 55. This number of mesh points used is sufficient to model accurately the heat transfer and fluid flow inside the hollow structure since the relative difference between the results does not exceed 0.5%. The grids utilized in this study are depicted in Fig. 5.

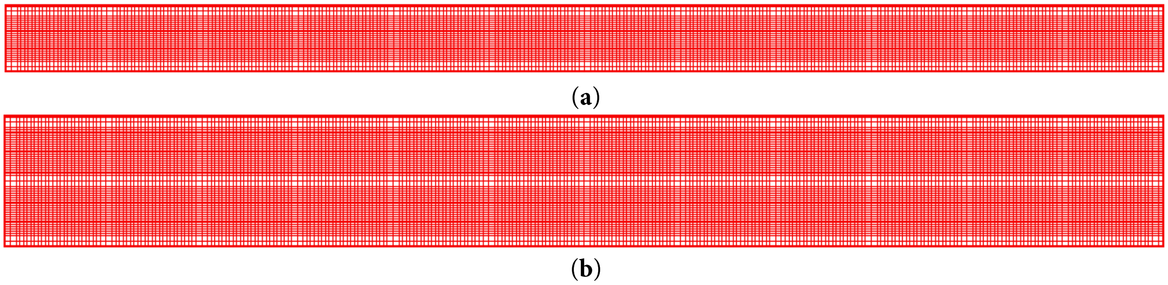

Figure 5: The grid sizes used for: (**a**) type 1 and (**b**) type 2.

Table 3: Effect of grid sizes on the overall heat flux at the active faces Q_e, Q_i and on streamline function Ψ_{max} for the hollow block type 1 (H1).

S (W/m²)	Grid	Q_o (W/m²)	Q_i (W/m²)	Ψ_{max}
S = 0	305 × 20	72.203	71.188	−0.054
	305 × 30	72.201	71.187	−0.054
	305 × 40	72.201	71.187	−0.054
S = 1000	305 × 20	251.883	250.225	0.205
	305 × 30	251.851	250.203	0.201
	305 × 40	251.851	250,203	0.201

Table 4: Effect of grid sizes on the overall heat flux at the active faces Q_e, Q_i and on the streamline function Ψ_{max} for the hollow block type 2 (H2).

	Grid	Q_o (W/m²)	Q_i (W/m²)	Ψ_{max}
S = 0	305 × 45	52.331	51.671	−0.00044
	305 × 55	52.310	51.640	−0.00044
	305 × 60	52.310	51.640	−0.00044
S = 1000	305 × 45	176.39	175.899	0.493
	305 × 55	176.311	175.823	0.485
	305 × 56	176.311	175.823	0.485

3.1 Impact of the Solar Irradiance

Isotherms and streamlines

The isotherms and the streamlines obtained for the two types studied and for the solar radiation (*S*), (a) S = 0 W/m^2 and (b) S = 1000 W/m^2 are illustrated in Figs. 6 and 7. The temperature field analysis indicates that the system primarily experiences heat transfer through conduction and radiation resulting from the heating from above. Indeed, the isotherms exhibit nearly parallel orientations within the holes. This quasi-horizontal stratification suggests a stable thermal layering where buoyancy forces are insufficient to trigger strong convective mixing, thereby maintaining the air's role as an effective thermal insulator. Distortions of the isotherms occur along the vertical solid walls due to the disparity in thermal conductivities between the solid and fluid mediums. In addition, we note that the increase in solar flux (S) does not affect the nature of the temperature fields for the two types of roofs 1 and 2 indicating that the conductive-radiative coupling remains the dominant heat transport mechanism even under high thermal loads.

Regarding the fluid flow structures in the hollow block cavities, it can be seen that the flow structures are practically similar and consist of 4 cells that rotate in opposite directions. These recirculation cells are generated by low-intensity flows, and when the solar flux increases the intensity of the flow increases (acceleration of the fluid in the cavities). Indeed, the maximum values of the current function Ψ_{max} are 0.00193 and 0.00631 for S = 0 W/m^2 and S = 1000 W/m^2 for the type 1 floor, and for the type 2 floor, the values of Ψ_{max} are 0.00577 and 0.0186 for S = 0 W/m^2 and S = 1000 W/m^2. Physically, the higher Ψ_{max} observed in Type 2 is attributed to the larger vertical expansion of its cavities, which allows for a slightly higher Rayleigh number. However, this increased fluid velocity does not translate to higher heat loss; rather, the reduction in the total volume of solid partitions (thermal bridges) in Type 2 and H5 configurations provides a superior global thermal resistance compared to the more fragmented Type 1. The thermal performance is thus a trade-off between convective intensity and solid-phase conduction, where the latter is the primary factor in the superiority of Type 2/H5 designs.

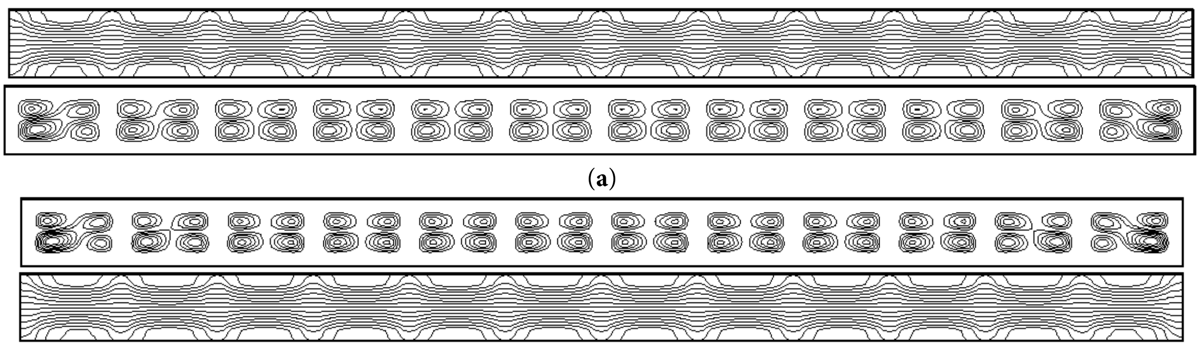

Figure 6: Isotherms and streamlines obtained for the roof (Type 1): (**a**) S = 0 W/m^2 (**b**) S = 1000 W/m^2.

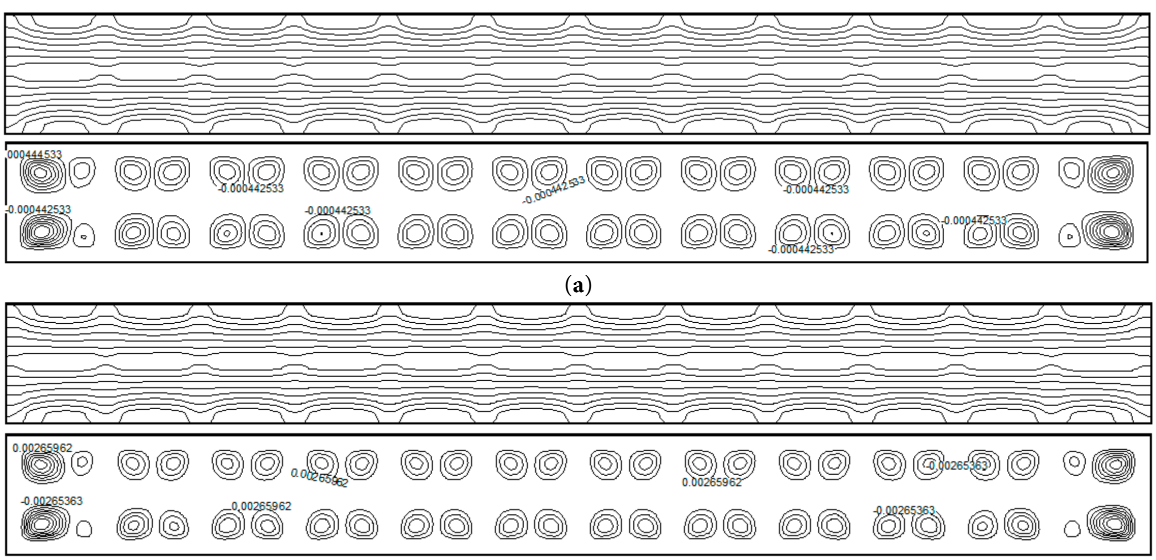

Figure 7: Isotherms and streamlines obtained for the roof (Type 2) for: (**a**) S = 0 W/m^2 (**b**) S = 1000. W/m^2.

Fig. 8 presents the isotherms and streamlines obtained for a solar irradiance of S = 1000 W/m^2 and a thermal conductivity of k_s = 1 W/mK, depicting the characteristics of the five different types of hollow blocks studied in this research. Notably, for hollow blocks of types H1, H2, H3, and H4, which feature a single cavity in the vertical direction (3 or 4 cavities), the flow structures within the cavities exhibit four cells rotating in opposite directions, displaying a qualitative symmetry (symmetry to the center). Furthermore, the maximum stream function values (Ψ_{max}) for H1, H3, and H4 are 0.201, 0.122, and 0.235, respectively. However, for the H2-type hollow block, the fluid acceleration is significant (Ψ_{max} = 0.501). This increase in flow intensity can be attributed to the larger cavity size, which allows for better fluid mobility through natural convection, providing more space for enhanced development. Conversely, in type H5, which has two cavities in the vertical direction (6 cavities), the flow consists of a pair of opposed cells with relatively low intensities (Ψ_{max} = 0.42304), accompanied by the formation of slight turbulence at the corners. Physically, the H5 configuration acts as a double thermal barrier. The presence of a horizontal solid partition between the top and bottom cavities interrupts the vertical buoyancy-driven flow, effectively segmenting the convective heat transport. This layering forces the heat to overcome two separate air-insulating zones, significantly reducing the overall thermal transmittance compared to the large, single-cavity designs like H2.

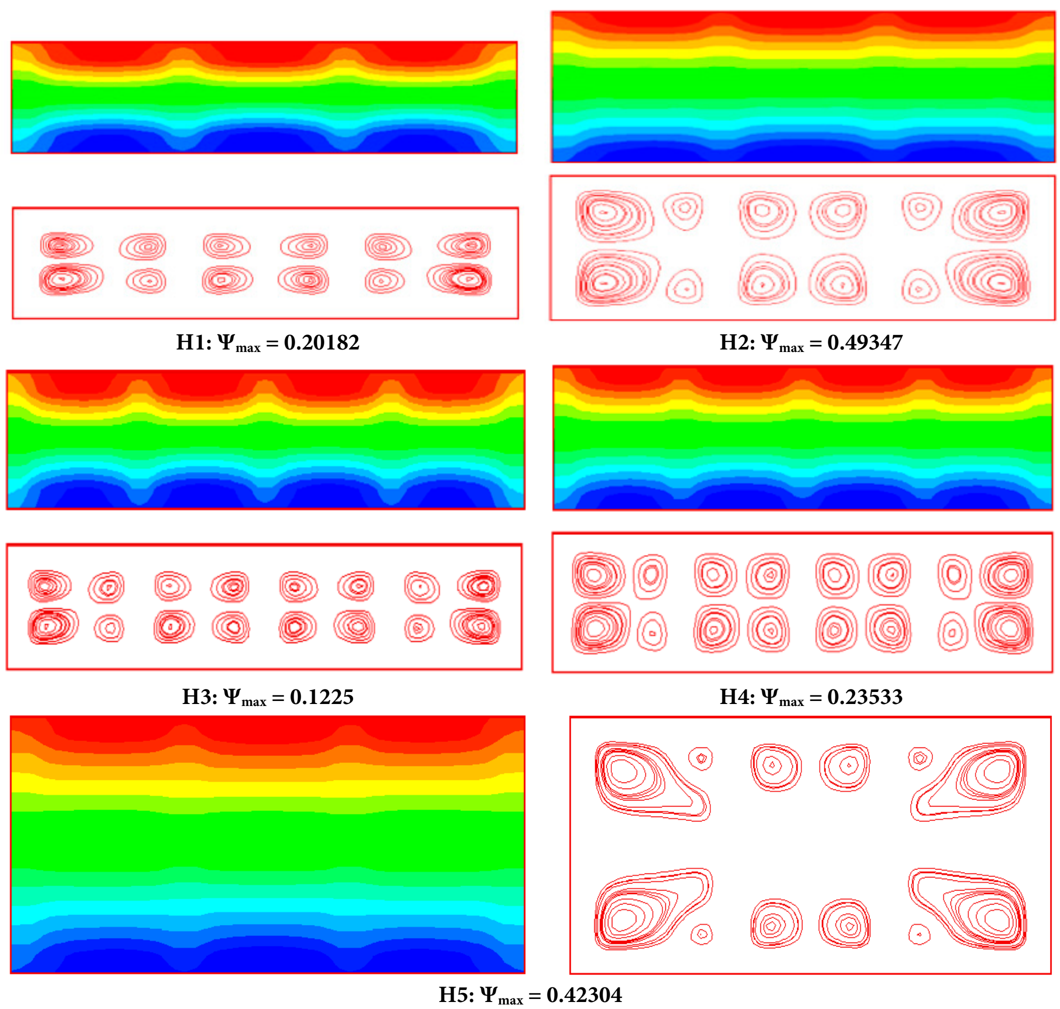

Figure 8: Isotherms and streamlines for S = 1000 W/m^2.

Upon analyzing the temperature field, it can be observed that, in all cases, the distortion of the isotherms is more pronounced in the vertical solid partitions. This can be attributed to the strong 2-dimensional nature of heat exchange through radiation and conduction, as well as the difference in conductivities between the fluid and solid media. In these vertical 'ribs', the solid phase acts as a thermal bridge, 'drawing' the heat downwards more rapidly than the air cavities. Additionally, the isotherms within the cavities appear as nearly parallel lines, perpendicular to the primary direction of heat transfer (Oy). This horizontal stratification confirms that within each individual cell, the air remains relatively stagnant, and the heat transfer is dominated by surface-to-surface radiation and gas-phase conduction rather than active convection, a state that is further stabilized in the H5 model due to the reduced vertical temperature gradient across each smaller cell.

Overall heat flux

Fig. 9 shows the evolution of the mean global heat flux Q as a function of the incident solar radiation S for the two types of roofs. As expected, Q increases with increasing S for both configurations. Despite the intrinsically nonlinear T^4 nature of the surface-to-surface cavity radiation, the two curves show an almost linear Q-S relation. This linearity is seen because the heat transfer through the solid walls dominates. The concrete matrix is the main thermal route, and its linearity according to Fourier's law dictates the overall response; the radiative exchange at the cavity level is a minor contributor for the range of irradiance values studied. Type 1 always has a higher heat flux than Type 2 for all values of S. Type 2 reduces the mean global heat flux by about 34% compared to Type 1, a significant improvement due to its geometric configuration. Type 2 reduces the density of vertical solid ribs, which are high-conductivity thermal bridges, forcing more heat to pass through the insulating air cells, thereby increasing the overall thermal opacity of the roof to solar heat gain. This advantage is further improved for the H5 block. The horizontal solid partition between two vertical levels of the cavity physically disrupts the buoyancy driven convective flow, creating two separate insulating air zones that increase the effective thermal path length and lead to heat flux reductions of up to 38% compared to single level configurations. Radiation effects and horizontal cell count are of secondary importance. The near-linear Q-S relationship confirms that cavity-level radiative exchange is subordinate to solid-partition conduction for all configurations. The qualitative flow topology is unaffected by the inclusion of a fourth horizontal hole. This geometric advantage is further improved by reducing the conductivity of the solid material to less than 1 W/mK, reducing the solid-bridge conductive contribution for all block types.

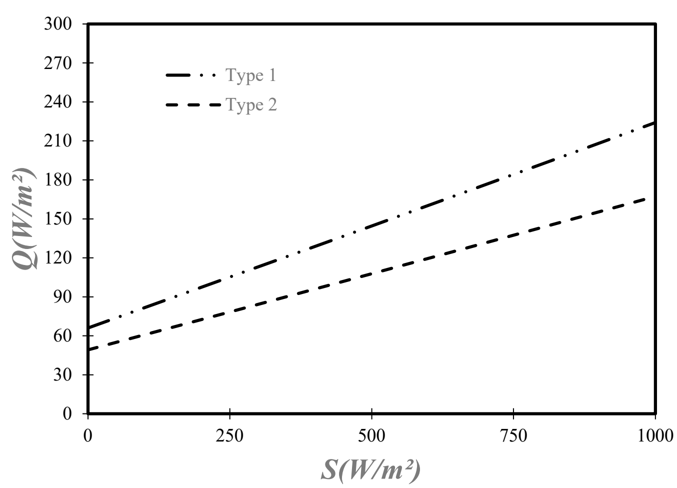

Figure 9: Evolution of the overall heat flux (Q) as a function of the solar radiation (S).

To have a more precise evaluation of the total heat transfer, the local heat flux distribution along the width X of the upper (hot) and lower (cold) horizontal surfaces is presented in Figs. 10 and 11 for S = 0 W/m^2 and S = 1000 W/m^2. The profiles for both surfaces are similar with peak values of heat flux at the solid partitions between the cavities. This is a direct consequence of the higher thermal conductivity of the solid material ks. The heat transfer in the cavities is much reduced as expected by the suppression of convection when the roof is heated from above by solar radiation. To more precisely estimate the total heat transfer, the local heat flux distribution along the width X of the upper (hot) and lower (cold) horizontal surfaces is presented in Figs. 10 and 11 for S = 0 W/m^2 and S = 1000 W/m^2. The profiles are similar for both surfaces with peak values of heat flux at the solid partitions between the cavities. This is directly related to the higher thermal conductivity of the solid material ks. The heat transfer in the cavities is, as expected, greatly reduced by the suppression of convection due to the heating of the roof from above by solar radiation.

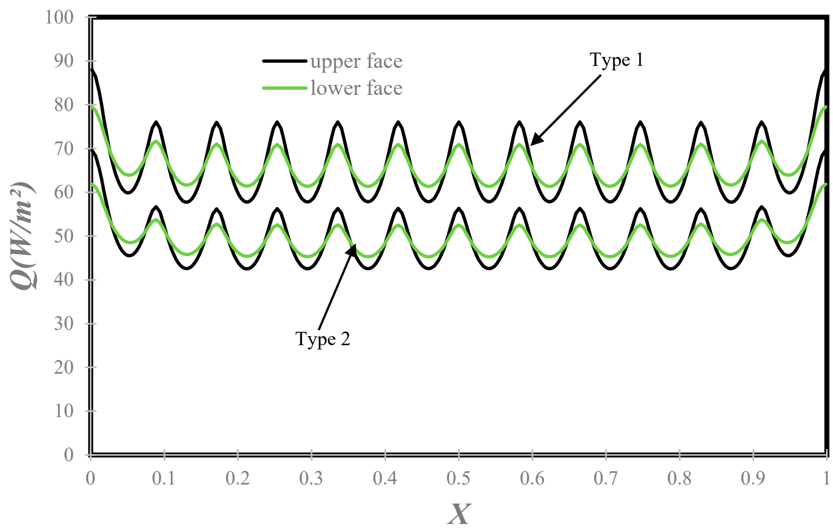

Figure 10: Evolution of the overall heat flux of the lower and upper faces for S = 0 W/m^2.

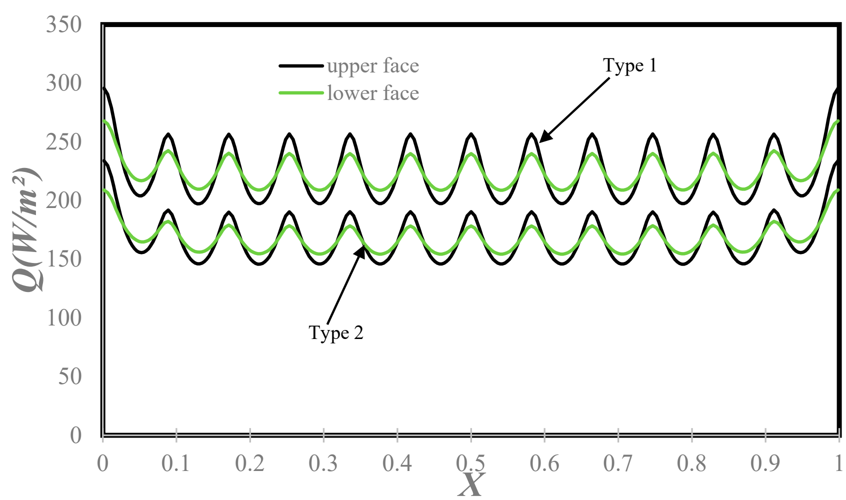

Figure 11: Evolution of the overall heat flux of the lower and upper faces for S = 1000 W/m^2.

The evolution of the average global heat flux (Q) through the analyzed configuration as a function of the incident solar flux (S) is presented in Fig. 12. For types H1, H2, H3, H4, and H5. As anticipated, the average heat flux (Q) increases with the incident solar flux (S). Despite the nonlinear nature of heat transfer by radiation, the obtained curves for all cases exhibit an almost linear relationship between Q and S. This linearity is primarily attributed to the dominant role of heat transfer by conduction along the solid partitions. It is worth noting that the heat flow crossing the H5 structure (with a total of 6 cavities) is significantly lower compared to the other types, namely H1, H2, H3, and H4 (with a total of 3 or 4 cavities). Specifically, the H5 structure reduces heat transfer by approximately 37.9% compared to the H3 structure and 33% compared to the H1 structure. These findings highlight the contribution of the H5 structure in enhancing the heat performance of the building's roof and confirm the need for solar protection of the roofs of the building, the sunniest to limit the increase in heat transfer.

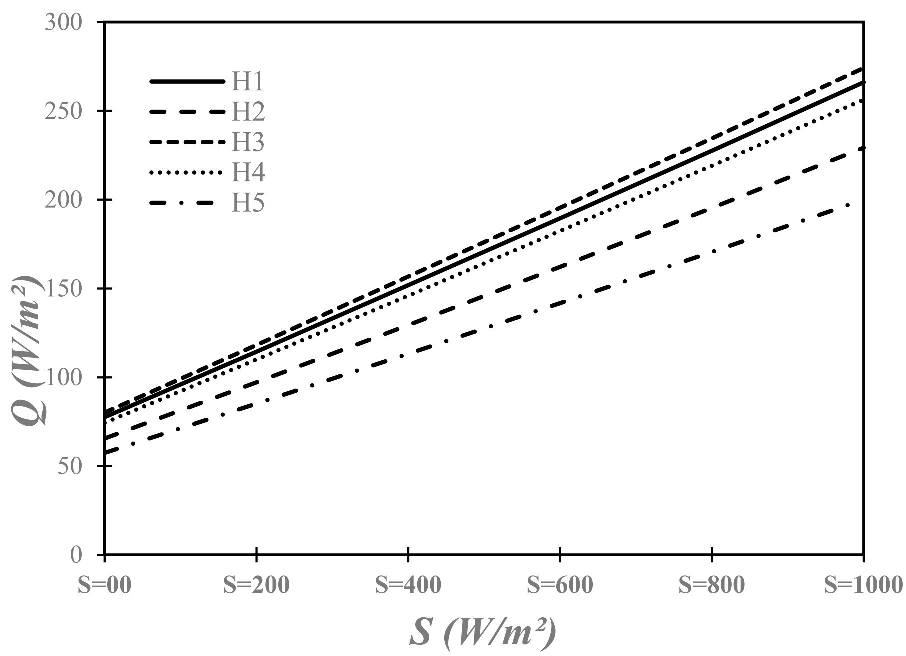

Figure 12: Evolution in the overall heat exchange as a function of the solar irradiance S.

Temperature variation

To examine the effect of the incident solar flux S on the temperatures of the external and internal faces of type 1 and type 2 roofs, Figs. 13 and 14 represent the temperature variation for S = 0 W/m^2 and S = 1000 W/m^2. As observed, the temperature profiles for both the outer and inner surfaces exhibit periodic characteristics with peaks occurring at the solid partitions separating the horizontal cavities. These maxima can be attributed to the significant conductive transfer along the vertical solid partitions, which act as thermal bridges, influencing the temperature values at these specific locations. It is worth noting that the calculated differences between the peak and minimum values are approximately 2%. The results depicted in Figs. 13 and 14 also demonstrate the substantial impact of the solar flux on the temperature of the external face Tse and the internal face Tsi of type 1 and type 2 roofs. Specifically, as S increases from 0 to 1000 W/m^2, the temperature Tse undergoes an increase of approximately 10.8% and 11.45% for roof types 1 and type 2, respectively, while the temperature Tsi experiences an increase of 5% for both wall types 1 and 2.

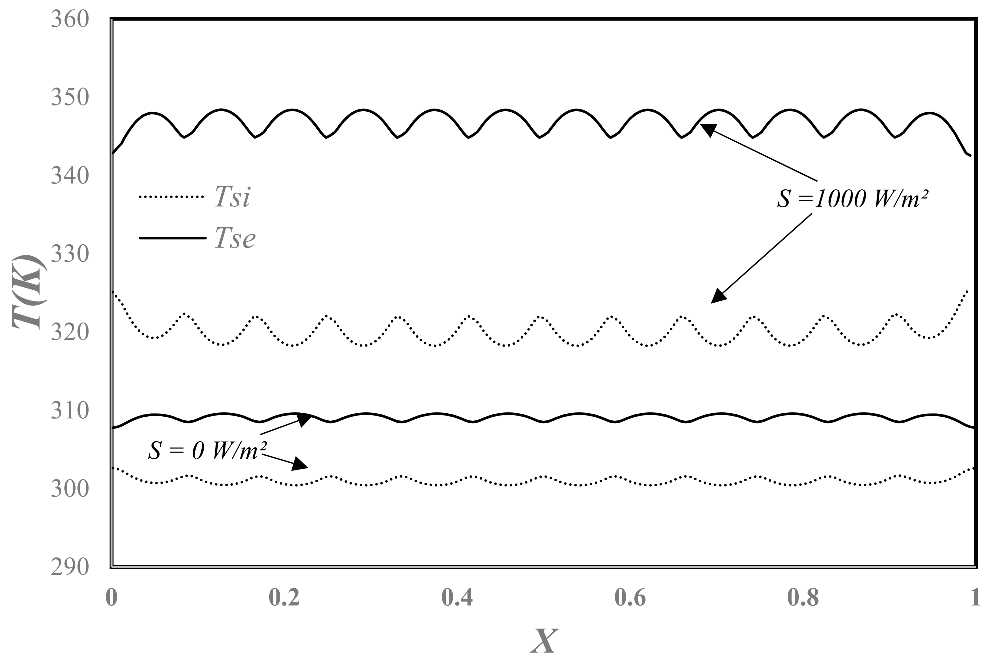

Figure 13: Temperature variation along the external and internal faces of the type 1 roof.

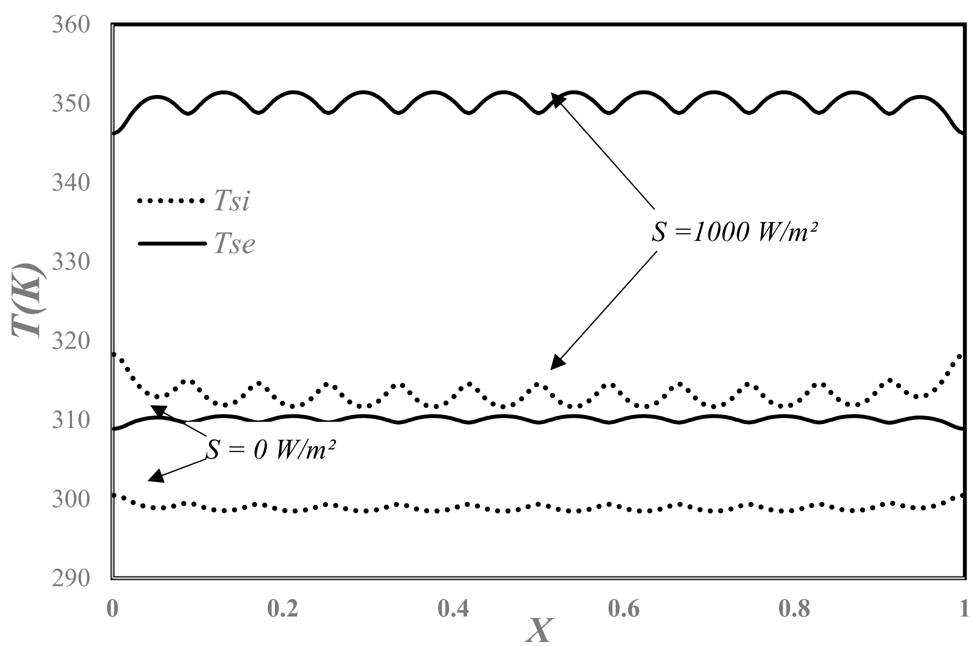

Figure 14: Temperature variation along the external and internal faces of the type 2 roof.

3.2 Effect of Heat Conductivity

The thermal conductivity of a material determines its ability to transfer heat, and it plays a vital role in the energy efficiency and heat performance of building components. To study the effect of this parameter (ks) on heat exchange across hollow blocks, Figs. 15–17 illustrate the average global heat flow (Q) across the examined configuration as a function of solar radiation (S) for three values of (ks): ks = 0.5 W/mK, ks = 1.0 W/mK, and ks = 1.5 W/mK. for the hollow blocks of types H1, H3, and H5, which differ in the number of. The analysis of Figs. 15–17 reveals a significant influence of the conductivity ks on the heat flow. Specifically, for solar radiation of S = 600 W/m^2, when the thermal conductivity (ks) varies between 0.5 and 1.5 W/mK, the heat flow (Q) experiences an augmentation of 22%, 21%, and 37% for the H1, H3, and H5 hollow blocks, respectively. This can be attributed to the increasing significance of conduction in the global heat exchange process as the conductivity (ks) rises. It is worth mentioning that the H5 hollow block type exhibits a significant reduction in heat flow in comparison to the other types, primarily due to the greater number of cavities in the vertical direction. These results demonstrate that the conductivity of the solid material in hollow blocks has a significant influence on the overall heat flow, particularly for values of ks greater than 1.

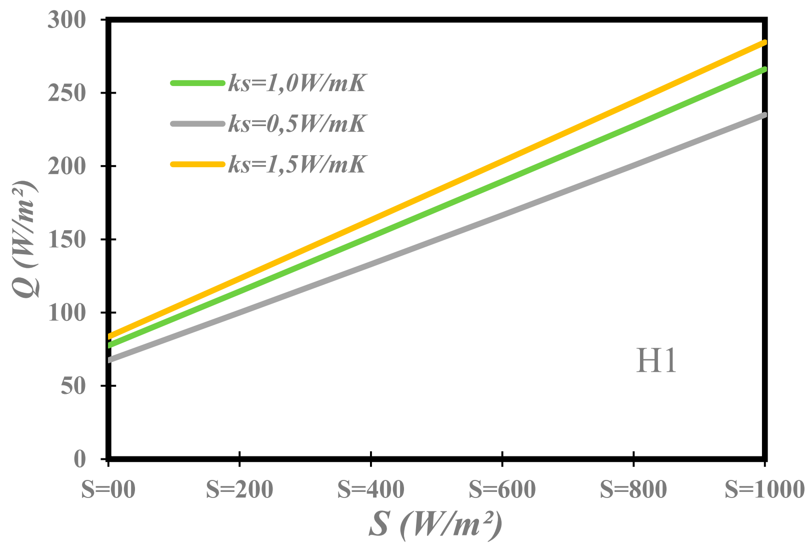

Figure 15: Effect of heat conductivity of type 1 (H1).

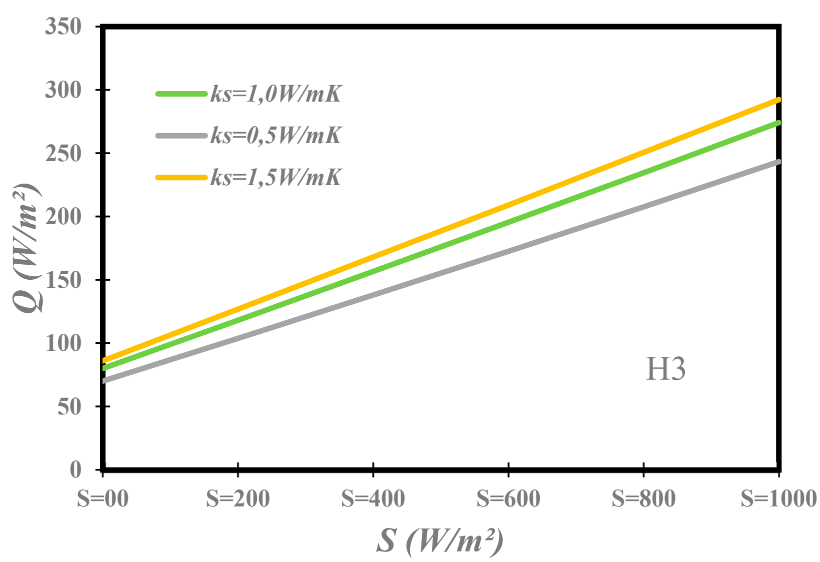

Figure 16: Effect of heat conductivity of type 3 (H3).

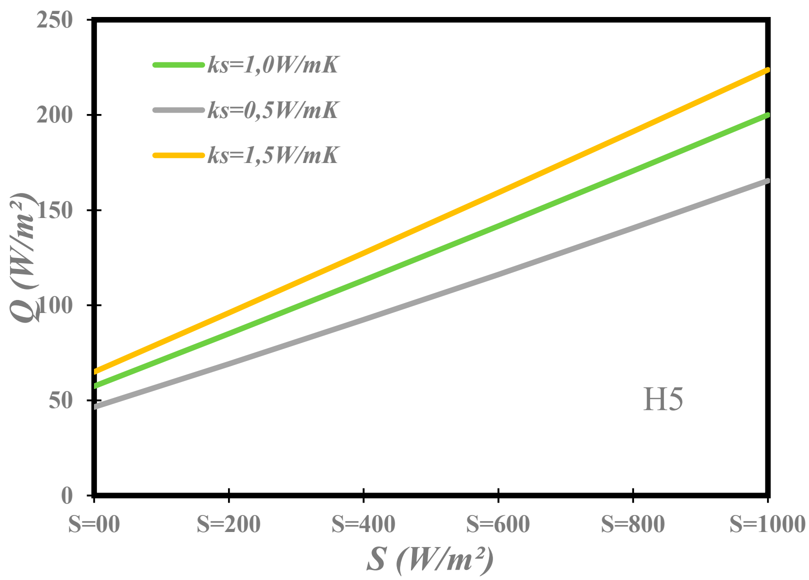

Figure 17: Effect of heat conductivity of type 5 (H3).

3.3 Impact of the Aspect Ratio of Internal Cavities

The roof construction units of the building differ in the aspect ratio of the interior cavity. The impact of the aspect ratio (A_r = h/l) on the global heat exchange across the examined roofs is depicted in Fig. 18. The findings indicate that the heat flow across both roof types is minimally influenced by the aspect ratio. When (A_r) changes from A_{r1} to A_{r2}, the heat flux reduces by approximately 10.8% and 16.17% for the type 1 roof and type 2 roof respectively. This effect can be attributed to the lower thermal conductivity of air compared to that of solid material. Increasing the aspect ratio of the hollow block cavity attenuates natural convection by promoting radiative heat exchange, resulting in a decrease in overall heat exchange across the roofs, particularly at high values of the incident solar flux (S). Analysis of these results demonstrates that employing hollow blocks with an aspect ratio of A_{r2} reduces heat transfer, thereby enhancing thermal resistance compared to using hollow blocks with an aspect ratio of A_{r1} in roof construction.

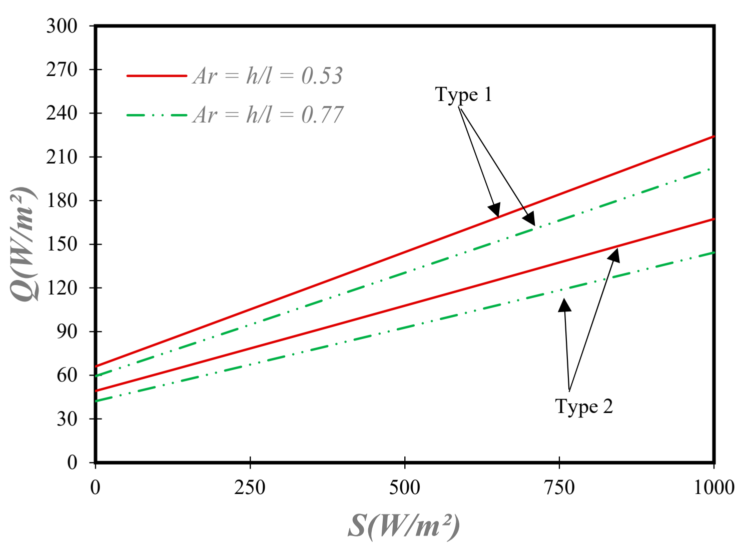

Figure 18: Impact of the aspect ratio on the global heat flux across both roofs of types (1) and (2).

4 Conclusion

This study investigates the combined heat transfer through hollow blocks with the most commonly used geometry and material in building roofs in hot-climate regions. A mathematical model is developed and used to investigate the influence of incident solar flux, the conductivity of the solid partitions, and the aspect ratio of hollow blocks on heat transfer and fluid flow. Our research reveals that the utilization of type 2 roofing can reduce the average heat flow by approximately 34% compared to type 1 roofing. Moreover, employing hollow blocks with an aspect ratio of Ar = 0.77 can minimize heat transfer loss and enhance the overall energy efficiency of buildings. It is noted that the impact of the number of holes in the horizontal orientation, such as types H1 and H2 (3 cavities), and types H3 and H4 (4 cavities) on the temperature field and flow structure remains negligible. The heat transfer across the various types of blocks studied significantly increases with an increase in the thermal conductivity of the block material. If structural constraints limit cavity number to ≤4, prioritize ks reduction below than 1 W/m·K; but if ks is fixed, optimize partition spacing to interrupt conductive paths. These insights hold practical implications for architects, engineers, and makers engaged in sustainable building design.

Acknowledgement: We would like to express our heartfelt gratitude to all those who contributed to this article.

Funding Statement: The authors received no specific funding for this study.

Author Contributions: Ayoube Baalla: Conceptualization, Writing—Original Draft. Thami Ait-Taleb: Writing—Review & Editing, Supervision. Mourad Najjaoui: Software. Hassan Chaib: Visualization, Methodology. All authors reviewed and approved the final version of the manuscript.

Availability of Data and Materials: The data supporting the findings of this study are available from the corresponding author, Ayoube Baalla, upon reasonable request.

Ethics Approval: Not applicable.

Conflicts of Interest: The authors declare no conflicts of interest.

References

1. Ministry of Energy Transition and Sustainable Development, Kingdom of Morocco. National energy consumption statistical reports [Internet]. Rabat, Morocco: Ministry of Energy Transition; 2023 [cited 2026 Jan 1]. Available from: https://www.mem.gov.ma.
2. Moroccan Agency for Energy Efficiency (AMEE). Energy efficiency guide in buildings [Internet]. Rabat, Morocco: AMEE; 2016 [cited 2026 Jan 1]. Available from: https://www.amee.ma.
3. Alvarado R, Xamán J, Hinojosa J, Álvarez G. Interaction between natural convection and surface thermal radiation in tilted slender cavities. Int J Therm Sci. 2008;47(4):355–68. [CrossRef].
4. Ait-Taleb T, Abdelbaki A, Zrikem Z. Numerical simulation of coupled heat transfers by conduction, natural convection and radiation in hollow structures heated from below or above. Int J Therm Sci. 2008;47(4):378–87. [CrossRef].
5. Boukendil M, Abdelbaki A, Zrikem Z. Detailed numerical simulation of coupled heat transfer by conduction, natural convection and radiation through double honeycomb walls. Build Simul. 2012;5(4):337–44. [CrossRef].
6. Hernández-Castillo P, Castillo JA, Huelsz G. Heat transfer by natural convection and radiation in three dimensional differentially heated tall cavities. Case Stud Therm Eng. 2022;40:102529. [CrossRef].
7. Miroshnichenko IV, Sheremet MA. Influence of thermal radiation on heat transfer through a hollow block. J Appl Comput Mech. 2023;9(2):419–29.
8. Gossard D, Lartigue B. Three-dimensional conjugate heat transfer in partitioned enclosures: Determination of geometrical and thermal properties by an inverse method. Appl Therm Eng. 2013;54(2):549–58. [CrossRef].

9. Sambou V, Lartigue B, Monchoux F, Adj M. Modeling of the thermal performance of air-filled partitioned enclosures: Effects of the geometry and thermal properties. J Build Phys. 2016;39(4):321–41. [CrossRef].
10. Majeed AH, Mahmood R, Liu D, Ali MR, Hendy AS, Zhao B, et al. Flow and heat transfer analysis over a pair of heated bluff bodies in a channel: Characteristics of non-linear rheological models. Case Stud Therm Eng. 2024;53:103827. [CrossRef].
11. Iqbal J, Akbar Y, Mouraya S. Aerothermal sensitivity and heat transfer analysis of hybrid nanofluid flow for solar-powered aircraft thermal management under realistic solar irradiance. Int Commun Heat Mass Transf. 2026;175:111211. [CrossRef].
12. Akbar Y, Iqbal J, Chen C. Numerical and ANN-based prediction of thermal enhancement in PTSC for solar-powered aircraft wings. Int Commun Heat Mass Transf. 2026;174:110933. [CrossRef].
13. Makinde AE, Makinde OD, Maaza M, Mokrani T. Thermal boundary layer of seawater desalination by distillation using CuS-infused selective porous solar absorber membrane. Multiscale Multidiscip Model Exp Des. 2025;8(10):444. [CrossRef].
14. Antar MA, Baig H. Conjugate conduction-natural convection heat transfer in a hollow building block. Appl Therm Eng. 2009;29(17–18):3716–20. [CrossRef].
15. Nouanegue HF, Muftuoglu A, Bilgen E. Heat transfer by natural convection, conduction and radiation in an inclined square enclosure bounded with a solid wall. Int J Therm Sci. 2009;48(5):871–80. [CrossRef].
16. Gao Y, He F, Meng X, Wang Z, Zhang M, Yu H, et al. Thermal behavior analysis of hollow bricks filled with phase-change material (PCM). J Build Eng. 2020;31:101447. [CrossRef].
17. Chihab Y, Essaleh L, Bouferra R, Bouchehma A. Numerical study for energy performance optimization of hollow concrete blocks for roofing in a hot climate of Morocco. Energy Convers Manag X. 2021;12:100113. [CrossRef].
18. Xamán J, Cisneros-Carreño J, Hernández-Pérez I, Hernández-López I, Aguilar-Castro KM, Macias-Melo EV. Thermal performance of a hollow block with/without insulating and reflective materials for roofing in Mexico. Appl Therm Eng. 2017;123:243–55. [CrossRef].
19. Jamal B, Boukendil M, El Moutaouakil L, Abdelbaki A, Zrikem Z. Numerical investigation of combined heat transfer through hollow brick walls. Eur Phys J Plus. 2020;135(10):813. [CrossRef].
20. Jamal B, Boukendil M, Abdelbaki A, Zrikem Z. Numerical simulation of coupled heat transfer through double solid walls separated by an air layer. Int J Therm Sci. 2020;156:106461. [CrossRef].
21. Bouchair A. Steady state theoretical model of fired clay hollow bricks for enhanced external wall thermal insulation. Build Environ. 2008;43(10):1603–18. [CrossRef].
22. Shi GZ, Li LP, Song CF, Cheng SM, Tao WQ, He YL. 3D numerical thermal optimization of the roofs constructed with cast-*in-situ* hollow concrete floor system by finite volume method. Energy Build. 2016;131:142–52. [CrossRef].
23. Morales MP, Juárez MC, Muñoz P, Gómez JA. Study of the geometry of a voided clay brick using non-rectangular perforations to optimise its thermal properties. Energy Build. 2011;43(9):2494–8. [CrossRef].
24. Sun J, Fang L. Numerical simulation of concrete hollow bricks by the finite volume method. Int J Heat Mass Transf. 2009;52(23–24):5598–607. [CrossRef].
25. Al-Tamimi AS, Al-Osta MA, Al-Amoudi OSB, Ben-Mansour R. Effect of geometry of holes on heat transfer of concrete masonry bricks using numerical analysis. Arab J Sci Eng. 2017;42(9):3733–49. [CrossRef].
26. Henrique dos Santos G, Fogiatto MA, Mendes N. Numerical analysis of thermal transmittance of hollow concrete blocks. J Build Phys. 2017;41(1):7–24. [CrossRef].
27. Najjaoui M, Ait-Taleb T, Abdelbaki A, Zrikem Z, Chaib H. Effect of hole configuration on heat transfer through a hollow block subjected to solar flux. Fluid Dyn Mater Process. 2022;18(5):1339–48. [CrossRef].
28. del Coz Díaz JJ, Nieto PJG, Sierra JLS, Biempica CB. Nonlinear thermal optimization of external light concrete multi-holed brick walls by the finite element method. Int J Heat Mass Transf. 2008;51(7–8):1530–41. [CrossRef].
29. del Coz Díaz JJ, García Nieto PJ, Betegón Biempica C, Prendes Gero MB. Analysis and optimization of the heat-insulating light concrete hollow brick walls design by the finite element method. Appl Therm Eng. 2007;27(8–9):1445–56. [CrossRef].
30. Sassine E, Cherif Y, Dgheim J, Antczak E. Experimental and numerical thermal assessment of Lebanese traditional hollow blocks. Int J Thermophys. 2020;41(4):47. [CrossRef].

31. Najjaoui M, Ait-Taleb T, Abdelbaki A, Zrikem Z, Chaib H. Coupled heat transfers in a three cavity hollow block subjected to an incident solar flux: Effect of heat conductivity. IOP Conf Ser Earth Environ Sci. 2018;161:012002. [CrossRef].
32. Zhang Y, Du K, He J, Yang L, Li Y, Li S. Impact factors analysis on the thermal performance of hollow block wall. Energy Build. 2014;75:330–41. [CrossRef].
33. Antoniadis KD, Assael MJ, Tsiglifisi CA, Mylona SK. Improving the design of Greek hollow clay bricks. Int J Thermophys. 2012;33(12):2274–90. [CrossRef].
34. Ouakarrouch M, Laaroussi N, Garoum M, Hajji A. Thermal performances assessment and improvement of hollow concrete blocks commonly used in Morocco: Experimental and numerical approach. J Therm Sci Eng Appl. 2022;14(10):101005. [CrossRef].
35. Noh-Pat F, Gijón-Rivera M, Zavala-Guillén I, Rivera-Solorio CI, May-Tzuc O, Shih MY. Thermo-energy performance of a phase change material integrated into lightweight hollow concrete roofs in warm–subhumid climate. Energy Build. 2024;312:114213. [CrossRef].
36. Shah SN, Khan R. Optimising thermal conductivity of insulated concrete hollow blocks in hot climates: Experimental–numerical investigation. Asian J Civ Eng. 2024;25(8):5955–73. [CrossRef].
37. Sambucci M, Sibai A, Fattore L, Martufi R, Lucibello S, Valente M. Finite element multi-physics analysis and experimental testing for hollow brick solutions with lightweight and eco-sustainable cement mix. J Compos Sci. 2022;6(4):107. [CrossRef].
38. Tian D, Zhang J, Gao Z. The advancement of research in cool roof: Super cool roof, temperature-adaptive roof and crucial issues of application in cities. Energy Build. 2023;291:113131. [CrossRef].
39. Structures et ouvrages d'art (hourdis) [Internet]. [cited 2026 Jan 1]. (In French). Available from: https://menaraprefa.ma/hourdis.
40. Siegel R, Howell JR. Thermal radiation heat transfer. 2nd ed. New York, NY, USA: Hemisphere Publishing Corporation; 1981.
41. Patankar SV. Numerical heat transfer and fluid flow. London, UK: Taylor & Francis; 1980.
42. Akiyama M, Chong QP. Numerical analysis of natural convection with surface radiation in a square enclosure. Numer Heat Transf Part A Appl. 1997;32(4):419–33. [CrossRef].
43. ASHRAE. Chapter 25: Heat, air, and moisture control in building assemblies fundamentals. In: 2021 ASHRAE handbook fundamentals (SI edition). Atlanta, GA, USA: American Society of Heating, Refrigerating and Air-Conditioning Engineers; 2021.